



**Abstract**

Alexeev A., Gorbalkov D., Kosako T. et. al. Optimization of Shielding Design for the Target Station of High Power Spallation Neutron Source: IHEP Preprint 98-43. – Protvino, 1998. – p. 11, figs. 7, tables 3, refs.: 21.

The shielding calculation for the high power spallation target on the base of KEK 3 GeV proton accelerator is presented. The Monte Carlo MOSKIT and HADRON codes were used to calculate particle yields from the W-target. The shielding analysis has been made by using the Sn-type ROZ6H code with the group cross section SADCO system. Problems of the best shield configuration for this facility are discussed.

**Аннотация**

Алексеев А., Горбатков Д., Косако Т. и др. Оптимизация защиты для мишенной станции мощного нейтронного источника на базе ускорителя: Препринт ИФВЭ 98-43. – Протвино, 1998. – 11 с., 7 рис., 3 табл., библиогр.: 21.

Выполнен расчет биологической защиты нейтронного источника от взаимодействия высокоинтенсивного протонного пучка с энергией 3 ГэВ с мишенью. Расчет выхода вторичных частиц при взаимодействии пучка с вольфрамовой мишенью выполнен с помощью двух монте-карловских программ MOSKIT и HADRON. Анализ ослабления излучения в защите основан на расчетах по одномерной программе РОЗ6Х с использованием многогрупповой системы констант Садко. Обсуждаются вопросы оптимальной конфигурации защиты для такого типа источника излучения.

## Introduction

Interest in radiation problems of high energy spallation neutron sources based on 1 MW proton beam power has grown, because there are several generations of the spallation neutron source projects: KEK [1],[2], ESS [3], ANL [4], BNL [5], LANL [6], ORNL [7], [8], PSI [9]. In case of high intensity particle beam, a careful analysis of shielding problems is needed. This paper presents the results of the shielding calculational investigation and the method of a shielding optimised for the 3 GeV proton target station in the neutron arena of JHP (Japan Hadron Project).

### 1. Computational methods

#### 1.1. Codes for a target and shielding simulation

The two Monte Carlo codes (HADRON and MOSKIT) were used for the target simulation. The one-dimensional discrete ordinate ROZ6H code was used to transport simulation in shielding with some configuration. The group cross section SADCO system was used for the calculation by MOSKIT and ROZ6H codes.

The Monte Carlo high energy transport HADRON code [10,11,12,13,14] is based on the cascade-exciton model (CEXM) of nuclear interactions. This model is the development of the cascade-evaporation model of nuclear reactions and is in a better agreement with experiments for secondary particle spectra, especially in the energy region below 100 MeV. In the inelastic interactions of hadrons with nuclei particles ( $n, p, \pi^0, \pi^\pm$ ) are generated in the program at the cascade stage of interaction, while  $n, p, d, t, {}^3\text{He}, \alpha$  and residual nuclei — at the de-excitation stage (which includes a preequilibrium decay as well as an equilibrium one).

The Monte-Carlo fast three-dimensional MOSKIT code [15,16] for the calculation of particles ( $n, p, \pi, \gamma$ ) transport was developed in IHEP. The simulation of particles trajectory in discrete phase volume space X, E, Z, F, I (I is the type of a particle) is the particularity of code, which determines its rapidly and universality. An energy region and particle type are determined by the constant's library. The transition matrix for hadrons is prepared on the base of the constant group file, which is produced by the SADCO

program complex used as a computational module. So, the code MOSKIT is assigned for the calculation functional of radiation fields.

The one-dimensional discrete ordinates transport ROZ6H code [15,17] is used for the attenuation calculation of neutrons, charged particles and secondary photons in a shield. The ROZ6H code is developed for the solution of multigroup kinetic equation of  $(n, p, \pi, \gamma)$  particle transport in the one-dimensional geometry by the discrete ordinates method for different sources, involving problems with fission and cascade processes.

The SADCO system [18] provides the transport calculation for neutrons (thermal  $<E < 10$  TeV), protons, pions, kaons (20 MeV  $<E < 10$  TeV), photons (0.01  $<E < 20$  MeV). The 66 neutron (49 below 20 MeV and 17 above 20 MeV) groups, 15 photon groups, 17 charged particle (protons and pions) groups are used in the calculations.

## 1.2. Calculation geometry

The shielding configurations of the target station are presented in Fig.1a,b,c. The first one is a common configuration which is used for high power spallation neutron sources [2] [3] based on proton accelerators. It consists of one layer of iron and one layer of concrete (Fig.1a). The radius of the target zone is 1 m. We don't take into account the equipment placed in the target zone. The thick layer of iron (the thickness of iron is equal to 4 up to 5 m for other spallation projects) is surrounded with concrete. The use of the iron shield allows one to decrease the size of the shield in comparison with the concrete one. On the other hand, our previous estimates has shown that the sandwich type of a shield is more suitable from the size and dose rate criteria. The second configuration (sandwich type) consists of two layers of iron and two layers of concrete (Fig.1b). A special investigation of an additional shield for neutron channels is needed. Fig.1c. presents the shield configuration for the beam neutron hole calculation. The radius of neutron beam hole is equal to 5.64 cm. The neutron channels are placed at some angles to proton beam direction. An additional cylindrical shields are placed around beam holes in the concrete shield. The purpose of this additional shield is to decrease the stream of nonscattered radiation from the target near the outlet of the neutron hole.

## 1.3. Input data for the shield design

Neutron is emitted by the cylindrical W-target bombarded with 3 GeV proton beam. An average beam intensity is 400 mA (1.2 MW). It corresponds to  $2.5 \cdot 10^{15}$  protons/s. The target size is 10 cm in diameter and 52 cm in length. The centre of the target is located in the centre of the target zone. The beam intensity shape used for the calculation is taken as gauss ( $I = \exp^{-r^2/(2 \cdot \sigma^2)}$ , where  $r$  is a radius from the target center ;  $\sigma = R/3$ ;  $R$  is the target radius). The size of the proton beam is equal to the target diameter. The composition and density of the shielding material are presented in Table 1.

The neutron flux-to-ambient dose equivalent ( $H^*(10)$ ) conversion factor specified by ICRP-51 was used for the neutron energy region below 20 MeV and by [14] for neutrons with energy above 20 MeV.

**Table 1.** Composition of concrete. Density of concrete and iron is equal to 2.3 and 7.8 gram.cm<sup>-3</sup>, correspondingly.

Atom	Weight (%)
H	1.01
C	0.10
O	53.57
Na	1.62
Mg	0.21
Al	3.43
Si	34.06
K	1.31
Ca	4.39
Fe	1.40

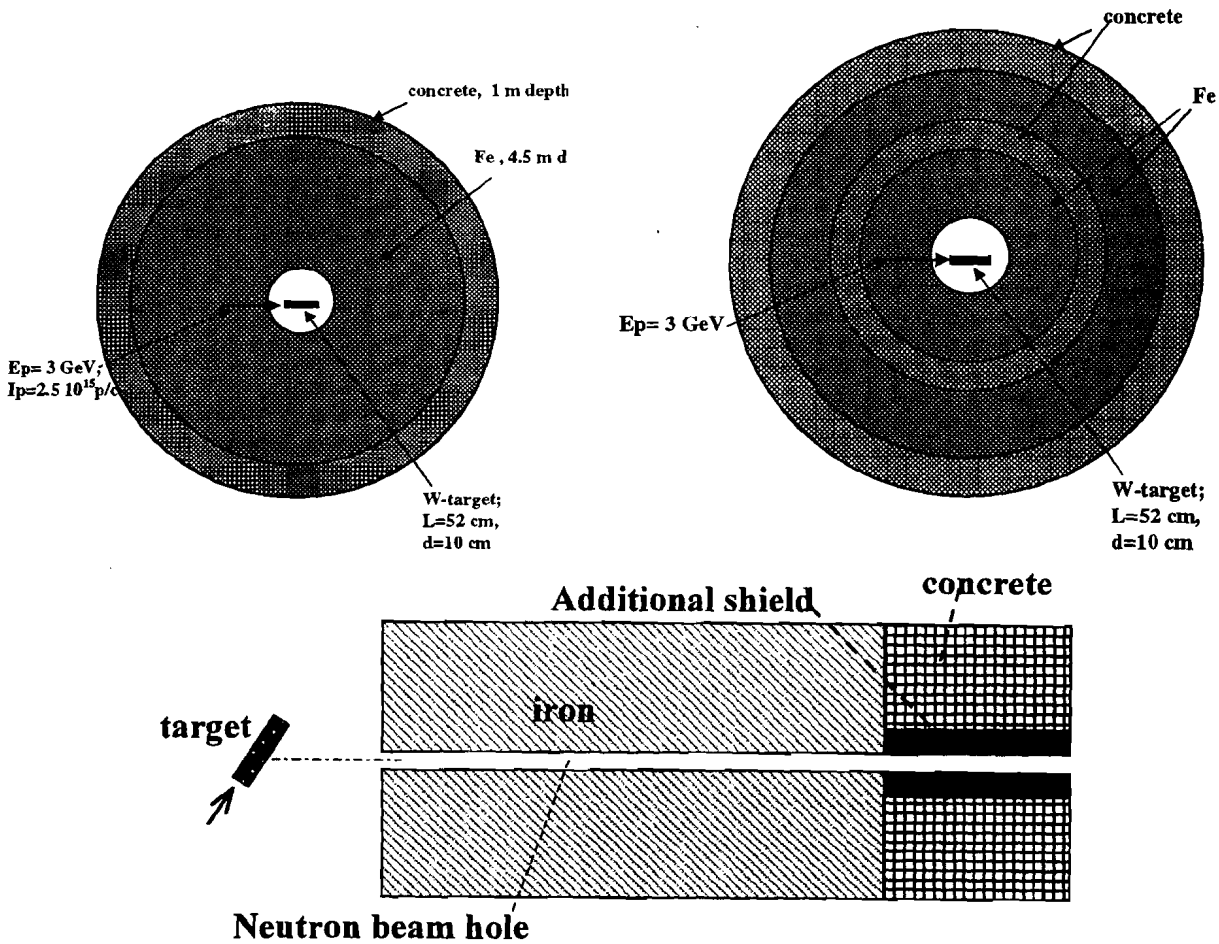


**Fig. 1.** Common geometry for the shield of the target station with ROZ6H code (a); sandwich shield geometry (b); calculation geometry of MOSKIT calculation for the additional shield of neutron beam hole (c).

## 1.4. Some remarks on the shield calculation

The point isotropic source was used for the one-dimensional ROZ6H code calculation. It was placed in the centre of the target zone. The spectra and yields of secondary particles (protons, neutrons, pions) of the point source were obtained with the 3-dimensional MOSKIT code calculation for the target. The spectrum and yield of particles were obtained for different polar angles in the proton beam direction by the MOSKIT calculation and at the 1 m distance from the target centre.

## 2. Result and discussion

### 2.1. Target simulation

The total yields of secondary particles which were calculated by the HADRON and MOSKIT codes are presented in Table 2. The main component are neutrons with the energy below 18 MeV. The difference between HADRON and MOSKIT calculation is not so great. Fig.2 presents a comparison between HADRON and MOSKIT codes calculation for the flux of secondary neutrons, protons, pions emitted from the W-target at different polar angles. The result of flux is presented for the 1 m distance from the target centre. The use of comparison between two codes can allow one to estimate systematical errors of the calculation. There is good agreement between HADRON and MOSKIT calculations for neutrons above 20 MeV and for pions. In the case of protons the MOSKIT result is higher than the HADRON one.

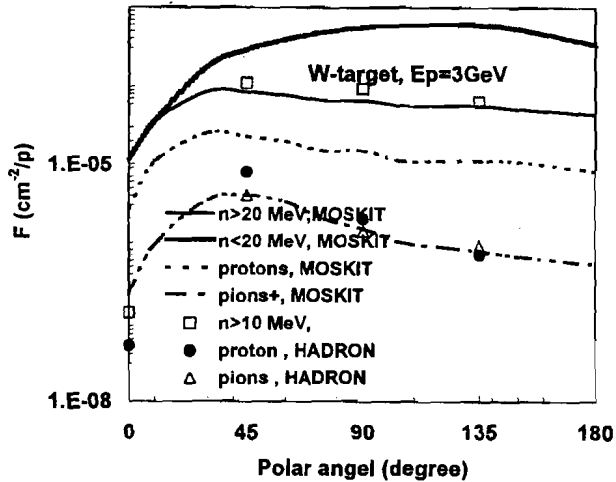


Fig. 2. Dependence of secondary particles flux from W-target from polar angle to proton beam direction; the lines are the MOSKIT code calculation, the symbols are the ADRON code one.

Table 2. Total yields of secondary particles (particles/proton).

Type	HADRON	MOSKIT
neutrons		
En > 10 MeV	10.71±0.05	-
En > 18 MeV	-	8.2±0.3
En < 18 MeV	-	60.0±1.2
protons	3.9	3.0
pions	2.1	1.1

Figs.3a,b,c present the secondary neutron spectra which were calculated by the HADRON and MOSKIT codes at 45, 90, 135° of the polar angles. There is agreement between both codes in an energy region below 300 MeV. In the case of neutrons with an energy above 300 MeV, there is the difference between two codes. It is explained by an analytical approximation of double differential cross sections, which is used in the SADCO system and by the use of a more suitable kinematical model in the HADRON code for this part of secondary neutron spectra. On the other hand, the contribution of neutrons with an energy above 300 MeV is neglected, so this source of a systematical error for the estimation of neutron dose equivalent rate behind the shield is neglected as well.

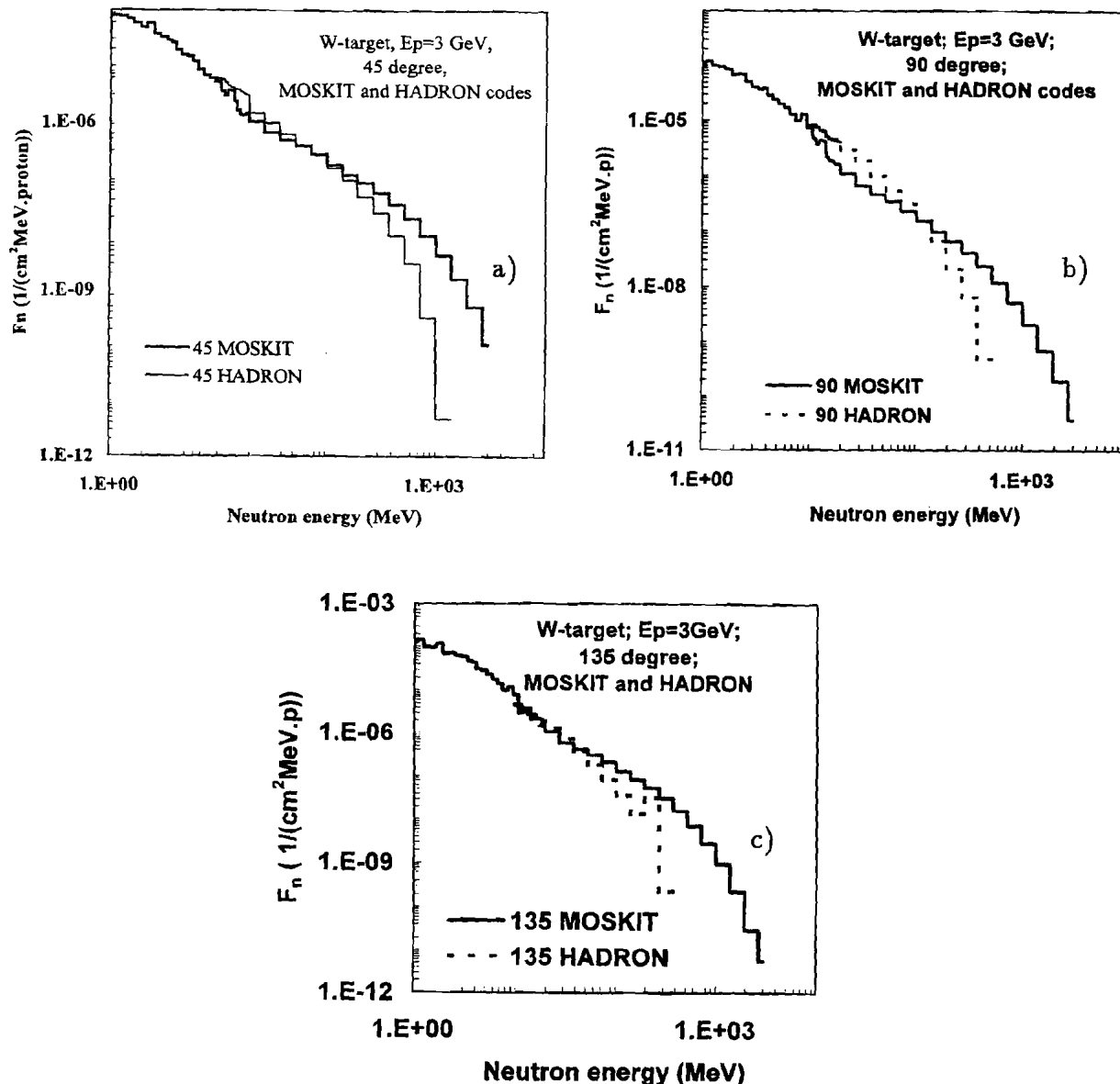


Fig. 3. Neutron spectra at the different polar angles at 1m to the W-target centre.

## 2.2. Shielding simulation

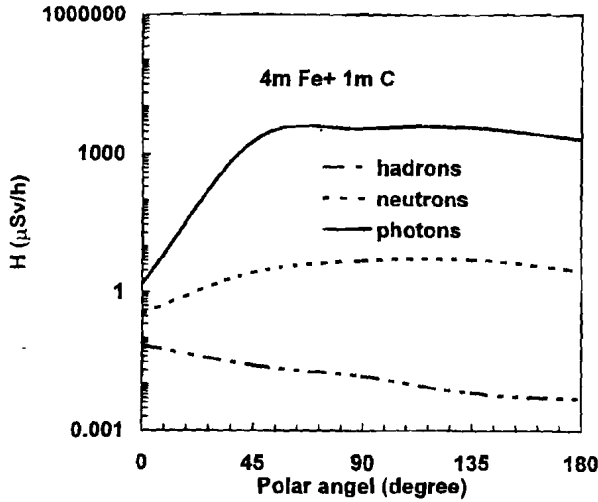


Fig. 4. Dose equivalent rate of hadrons, neutrons and photons inside of the iron-concrete shield.

varied to obtain more suitable configuration based on the criterion of size and attenuation. The relative dependence of dose equivalent rate on a polar angle is the same for different shield configurations, so the dose equivalent rate for polar angle  $90^\circ$  (maximum of dose rate) is shown in Table 3. In the case of iron-concrete shield the photons are the main component of total dose equivalent rate. In the case of sandwich configuration a relative contribution of neutrons and photons varies with iron and concrete thickness combination. If the thickness of the first iron layer is higher than 0.2 m, then neutron dose equivalent rate is higher than photon one. Neutron and photon dose equivalent rate decreases with the thickness of the first iron layer. On the other hand, the decreasing of iron thickness lead to the increase of hadron dose equivalent rate. Fig.5 shows the effect of sandwich configuration on the decreasing of neutron and photon dose equivalent. Dependencies of neutron flux with energy below and above 20 MeV, charge particles flux (protons and pions), thermal neutron and photon flux from shield depth are presented for two shield configurations: 4 m iron + 1 m concrete and 2.5m iron + 0.3 m concrete + 0.7 m iron + 1 m concrete. In the first case such high contribution of photons is explained by captured photons in the iron (which is not enough attenuation with 1 m concrete) and photons from capturing thermal and intermedium neutron in the concrete which stream through iron without attenuation. In the other case the first concrete layer attenuate thermal and intermediate neutrons which reach the first iron layer; the second iron layer decreases captured photons which are generated in the first concrete layer. In the first case the decreasing total thickness of iron increases hadron dose equivalent rate by a factor of 3, but photon dose rate decreases by a factor of about  $10^4$  and the total dose equivalent rate decreases by  $10^3$ .

Fig.4 presents the dose equivalent rate of hadrons (protons and neutrons with an energy above 20 MeV), neutrons with an energy below 20 MeV and photons inside (on the surface of the concrete shield) the common iron-concrete shield configuration (4 m Fe + 1 m concrete) at different polar angles. The maximum of neutron and photon dose is between  $90$  and  $135^\circ$ . The maximum of hadrons dose is in the proton beam direction near  $0^\circ$  of the polar angle.

The dose equivalent rate of different radiation components is presented in Table 2. The calculational results are presented for different types of the shield configurations: two layers (iron + concrete) and the sandwich type (iron + concrete + iron + concrete). The depth of iron and concrete was

Table 3. Dose equivalent rate of hadrons, neutrons, photons inside the shields with the different configuration.

Shield configuration	hadrons ( $\mu\text{Sv/h}$ )	neutrons ( $\mu\text{Sv/h}$ )	photons ( $\mu\text{Sv/h}$ )	total ( $\mu\text{Sv/h}$ )
1) 4m Fe +1 m C	0.0261	2.73	1893	1896
2) 4.5mFe+1mC	0.00059	0.731	510	511
3) 2.5 m Fe +2m C	12.7	7.1	165	185
4) 2.5mFe+0.1mC+0.9mFe+1mC	0.49	0.47	138	139
5) 3mFe+0.2mC+0.8mFe+1mC	0.04	2.2	1.1	3.34
6) 2.5mFe+0.3mC+0.7mFe+1mC	1.03	0.6	0.22	1.85

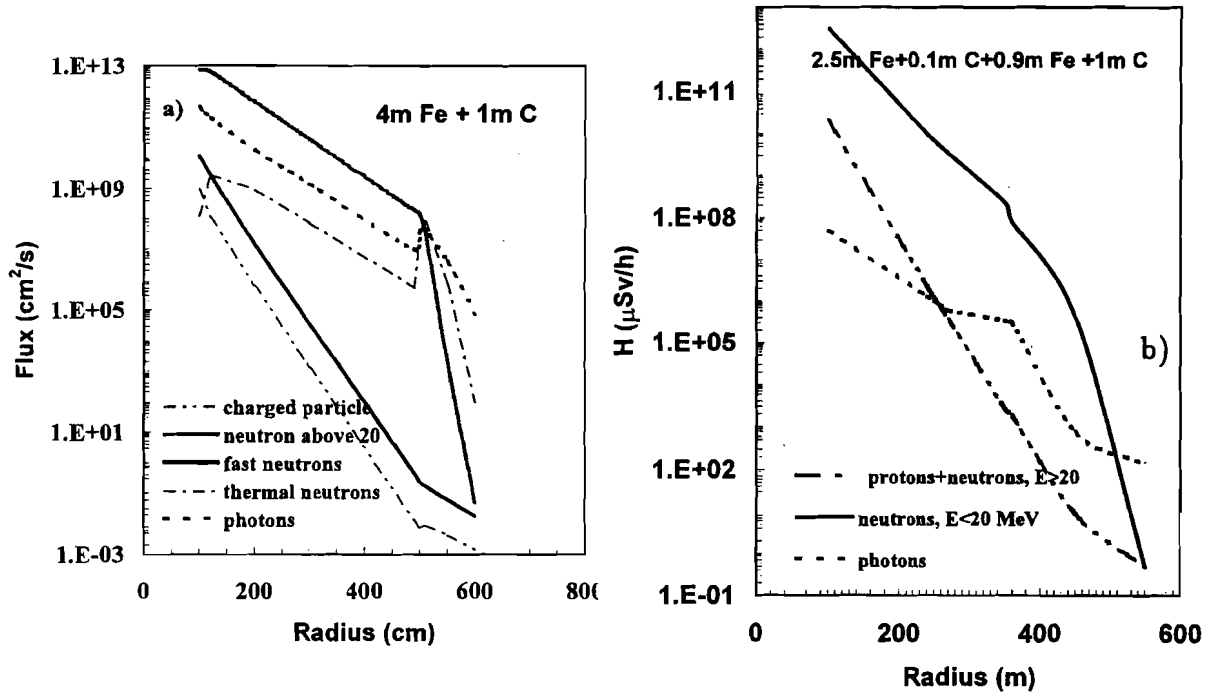


Fig. 5. Particle flux at the different distance from the target centre for the common (a) and sandwich (b) shield configuration.

In case of using the criteria: a minimum shield size, a minimum shield weight, a minimum dose equivalent rate, then this shield configuration is a compromise for the shielding design.

In case of the common shield the photon dose equivalent rate is higher than the restricted dose rate level ( $3 \mu\text{Sv/h}$ ). With of the sandwich shield configuration the photon dose equivalent rate is not so high, and total dose equivalent rate is less than the restricted level for configuration 6 (2.5 m Fe + 0.3 m C + 0.7 m Fe + 1 m C). The size for the common shield configuration was obtained by engineering calculation based on the attenuation length method that estimated only neutron dose equivalent rate only. This estimation [2] agrees with the present data, for the example, the estimations of neutron dose equivalent

are 2.9 for [2] and  $2.8\mu\text{Sv/h}$  for the present calculation. But, on the other hand, there is the engineering method based on attenuation length [19] to estimate the dose rate of secondary photons in the case of iron-concrete or iron-water-shield.

### 2.3. Beam hole simulation

The additional source of radiation behind the shield are neutron channels. The additional shield is needed to decrease primary radiation around the beam hole.

The calculation of dose equivalent rate around the beam hole was carried out with the MOSKIT code for the iron+concrete shield (4.5 Fe+1m C). Fig.6a,b,c presents the dose equivalent rate around the beam hole inside the shield for different additional shield materials (concrete, iron, polyethylene). The additional shield is the cylinder 30 cm in diameter and 1 m long. At first sight iron is a more suitable material to stop nonscattered radiation from the beam hole. But the result shows that the contribution of nonscattered component of radiation is not significant at the distance from the beam hole centre above 10 cm. Such behaviour does not depend on the material of the additional shield. In the case of iron the nonscattered component is stopped, but the scattered component is much higher than for polyethylene and concrete. It has been explained that iron is well penetrable for neutron with energy below 20 MeV. So, iron as material of the additional shield has no advantages over concrete. The calculation was carried out for the distances up to 40 cm of the distance from the hole centre, because the Monte Carlo calculation takes a long run-time of a computer.

In this case the engineering method may be used, which allows one to estimate that 2 m concrete shield around the beam line reduces the dose equivalent rate to the restricted level.

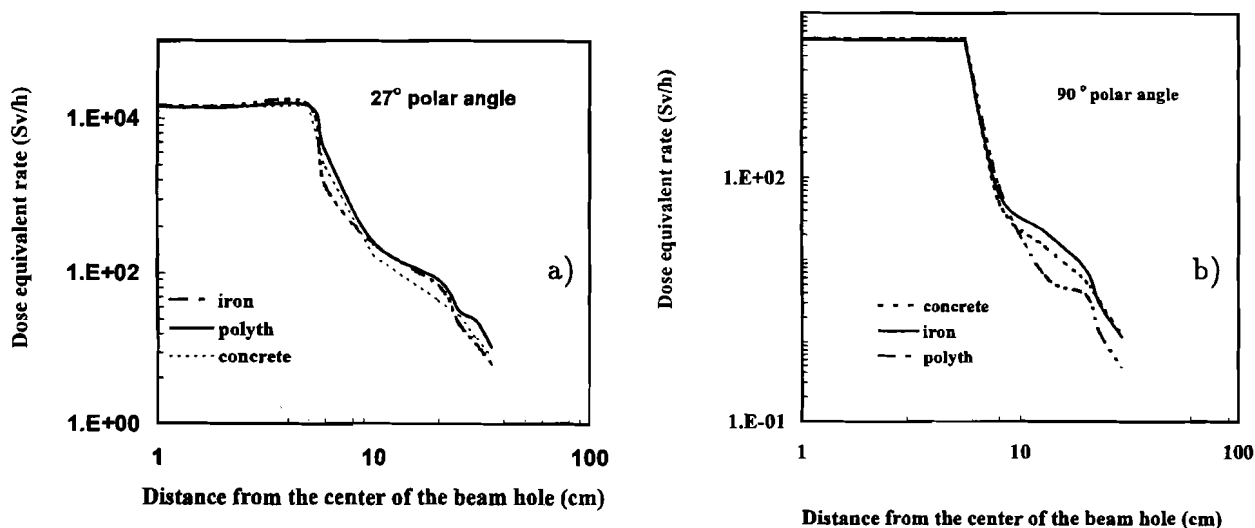


Fig. 6. Dose equivalent rate around the beam hole with different material of the additional shield at the polar angle of  $45^\circ$  (a) and  $90^\circ$  (b).

## 2.4. Systematical errors of the calculation

There are some sources of systematic errors for the calculation of dose equivalent rate:

### A. Estimation of secondary particles yields from the target.

The calculational neutron yield with the energy above 10 MeV obtained with both codes agrees within  $\pm 30$  percent. Fig.7 presents the neutron dose equivalent rate of a high energy part of neutron spectra from the target to dose equivalent rate behind the iron spherical shield with 4 m thickness at  $90^\circ$  of polar angle:

$$H(E_n) = I_p / (R^2) \int_{E_n}^{3\text{GeV}} F(E) h(E) \cdot e^{-d/\lambda(E)} dE, \quad (1)$$

where  $F(E_n)$  is the neutron flux at 1 m from the isotropic source;  $d$  is the shield thickness (4m);  $R$  is the distance from point source to the point (5 m);  $\lambda(E_n)$  is the neutron dose equivalent attenuation length for iron [20];  $h(E_n)$  is the flux-to-dose equivalent conversion factor;  $I_p$  is the proton current. The value of  $H(E_n)$  was calculated with MOSKIT and HADRON data of  $F(E_n)$ . The difference between MOSKIT and HADRON data for  $H(E_n > 10 \text{ MeV})$  is less than 50 %. In the case of energy region above 100 MeV the difference between two codes is very high. On the other hand, the difference in high energy region for the secondary neutron spectra do not reach a high systematical error of dose rate behind the iron shield because the contribution of this part to the total dose equivalent rate is less than  $\pm 30$  %. So, the neutron dose equivalent rate calculation with MOSKIT code of neutron spectra from the target is the overestimation with the errors less than 50 %. The difference in the secondary proton yield does not result in a significant error of dose rate because the contribution of protons to a total secondary particle flux is less than 10 percent.

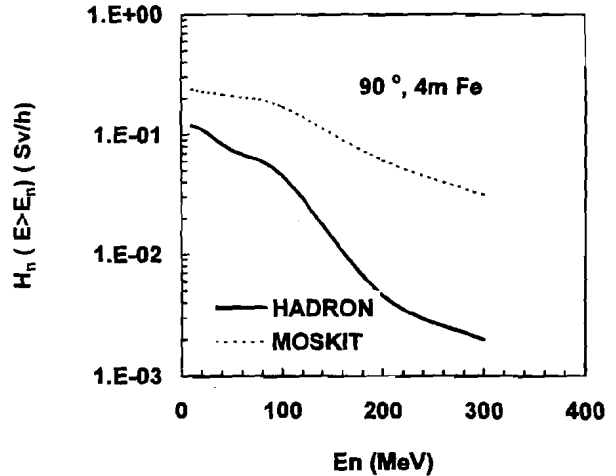


Fig. 7. The neutron dose equivalent rate for neutron with energy above  $E_n$ . Neutron spectra from the target was calculated with MOSKIT and HADRON codes. Shielding thickness is 4m Fe.

### B. Calculation geometry.

The isotropic source was used in one-dimensional shield calculation. Because the angular distribution of a secondary particle is not isotropical, the value of dose equivalent rate behind the shield may be overestimated in the case of the strong direction of dose rate ( $90^\circ$  of polar angle). Because the shield size was chosen due to the maximum of dose equivalent rate, so our estimation of shield is the overestimation. The estimation of a potential error can be obtained by a comparison of the attenuation length calculation for

two geometries: planar ( normal-incident parallel beam) and spherical ( isotropic source). The results [20] of comparison of different shield codes show that in the first case the attenuation length is higher by 5-8 %.

### C. Attenuation of radiation.

The comparison of some shielding codes [20] show that the attenuation length of iron obtained with the codes may differ by 100%. The calculational result depends on the used cross sectional library. The evaluation of neutron attenuation length for iron will be the topic of a separate investigation. But, on the other hand, our estimation of neutron attenuation length ( $300\text{-}320 \text{ g/cm}^2$ ), which was obtained by this calculation, is a conservative estimate for a shielding design.

## Conclusion

The calculation analysis of the shield for the 3 GeV proton high power spallation source was performed. The comparison of two different codes (HADRON and MOSKIT) shows that there is the agreement between the calculatal result of secondary particle spectra and yields from the W-target. The calculation of dose equivalent rate inside the shield shows that in the case of iron-concrete shield photons are the main component. The sandwich (iron-concrete-iron-concrete) shield is preferable for such shield facility, this configuration allows one to decrease the level of dose equivalent rate with the use of the same size of a shield. This phenomenon ( high photon level of dose rate ) is not usually taken into account for a shielding design based on the simple attenuation length calculation, on the other hand, this calculation result is needed for an experimental verification.

The authors are grateful to T.Sakaya, L.A.Lebedev, S.G.Mikheenko for help in our work.

## References

- [1] M.Furusaka et al., Proc. ICANS-XIII, PSI Proceeding SF02 (1995) pp.836-842.
- [2] M.Furusaka et al., KEK Report 96-4, 1996.
- [3] D.Filges et al., private communication, Material of SATIF3 Meeting, Tohoku University, Sendai, Japan, May 12-13, 1997.
- [4] J.M.Carpenter, Proc. ICANS-XIII, PSI -Proceeding 95-02 (1995), pp. 777-797 or ANL Report ANL-95/13 (1995).
- [5] Y.Y. Lee et al, Proc. ICANS-XIII, PSI- Proceeding 95-02 (1995), pp.802-807. or H.Ludewing et al, Proc. ICANS-XIII, PSI- Proceeding 95-02 (1995), pp.808- 811
- [6] N.Bultmanu et al., Report LAA-UR-95-4300 (1995) or R.Pynn and D.Weinacht, Proc. ICANS-XIII, PSI — Proceeding 95-02 (1995), pp.798-802
- [7] P. Appleton, Proc. ICANS-XIII, PSI- Proceeding 95-02 (1995),pp. 814-818

- [8] T.A.Gabriel et al., private communication, Material of SATIF3 Meeting, Tohoku University, Sendai, Japan, May 12-13, 1997.
- [9] G.S. Bauer, IAEA Vienna TECDOC-836 (1995) pp.97-114.
- [10] V.T.Golovachik, V.N.Kustarjov, V.N.Lebedev, E.N.Savitskaya and A.V.Sannikov. Dose Conversion Factors for Neutrons from Thermal to 20 MeV and for Protons from 2 to 600 MeV. Proc. of the 10th Conf. on Charged Particle Accel. Dubna (1987) pp.411-414.
- [11] V.T.Golovachik, V.N.Kustarjov, E.N.Savitskaya and A.V.Sannikov. Absorbed Dose and Dose Equivalent Depth Distributions for Protons with Energies from 2 to 600 MeV. Radiat. Prot. Dosim. **28** (3) 189-199 (1989).
- [12] E.N.Savitskaya and A.V.Sannikov. High Energy Neutron and Proton Kerma Factors for Different Elements. Radiat. Prot. Dosim. **60**(2), 135-146 (1995).
- [13] A.V.Sannikov and E.N.Savitskaya. Ambient Dose and Ambient Dose Equivalent Conversion Factors for High Energy Neutrons. CERN Preprint CERN/TIS-RP/93-14 (1993).
- [14] A.V.Sannikov and E.N.Savitskaya. Ambient Dose Equivalent Conversion Factors for High Energy Neutrons Based on the New ICRP Recommendations. Proc. of the 8th Symposium on Neutron Dosimetry, Paris(1995).
- [15] D.V.Gorbatkov, V.P. Kruchkov, O.V.Sumaneev, Program Complex for High Energy Hadron Transport Calculation to Solve Radiation Problems in Accelerators. Preceding of the Fourth European Particle Accelerator Conference. EPAC 94. Vol. 3, pp.2588, Word Scientific Publ. Co. Pte. Ltd., London, 1994.
- [16] V.P.Kruchkov et. al. IHEP Preprint 92-132- Protvino, 1992. (in Russian).
- [17] A.E.Averin et. al., Proc. Top Mtg. Adv. in Mathem. Cmput. and Reactor Physics, Pitts- burgh, USA (1991) Vol. 5.
- [18] D.Gorbatcov, V.Kryuchkov. SADCO-2 : a modular code system for generating coupled nuclear data libraries to provide high-energy particle transport calculation by multigroup methods. NIM A 372 (1996) 297-301.
- [19] H.Kotegawa, Y.Sakamoto, S.Tanaka, JAERI-DATA/CODE 95-004, 1995.
- [20] H.Hirayama, *Inter-comparison of the Medium-Energy Neutron Attenuation in Iron an Con- crete*, private communication, Material of SATIF3 Meeting, Tohoku Japan, May 12-13, 1997.
- [21] Gorbatkov D., private communication , IHEP, 1997.

Received June 9, 1998

А.Алексеев, Д.Горбатков, Т.Косако и др.

Оптимизация защиты для мишенной станции мощного нейтронного источника на базе ускорителя.

Оригинал-макет подготовлен с помощью системы  $\text{\LaTeX}$ .

Редактор Е.Н.Горина.

Технический редактор Н.В.Орлова.

---

Подписано к печати 16.06.98. Формат 60 × 84/8. Офсетная печать.

Печ.л. 1,37. Уч.-изд.л. 1,05. Тираж 180. Заказ 296. Индекс 3649.

ЛР №020498 17.04.97.

---

ГНЦ РФ Институт физики высоких энергий  
142284, Протвино Московской обл.

Индекс 3649

---

ПРЕПРИНТ 98-43,            И Ф В Э,            1998

---